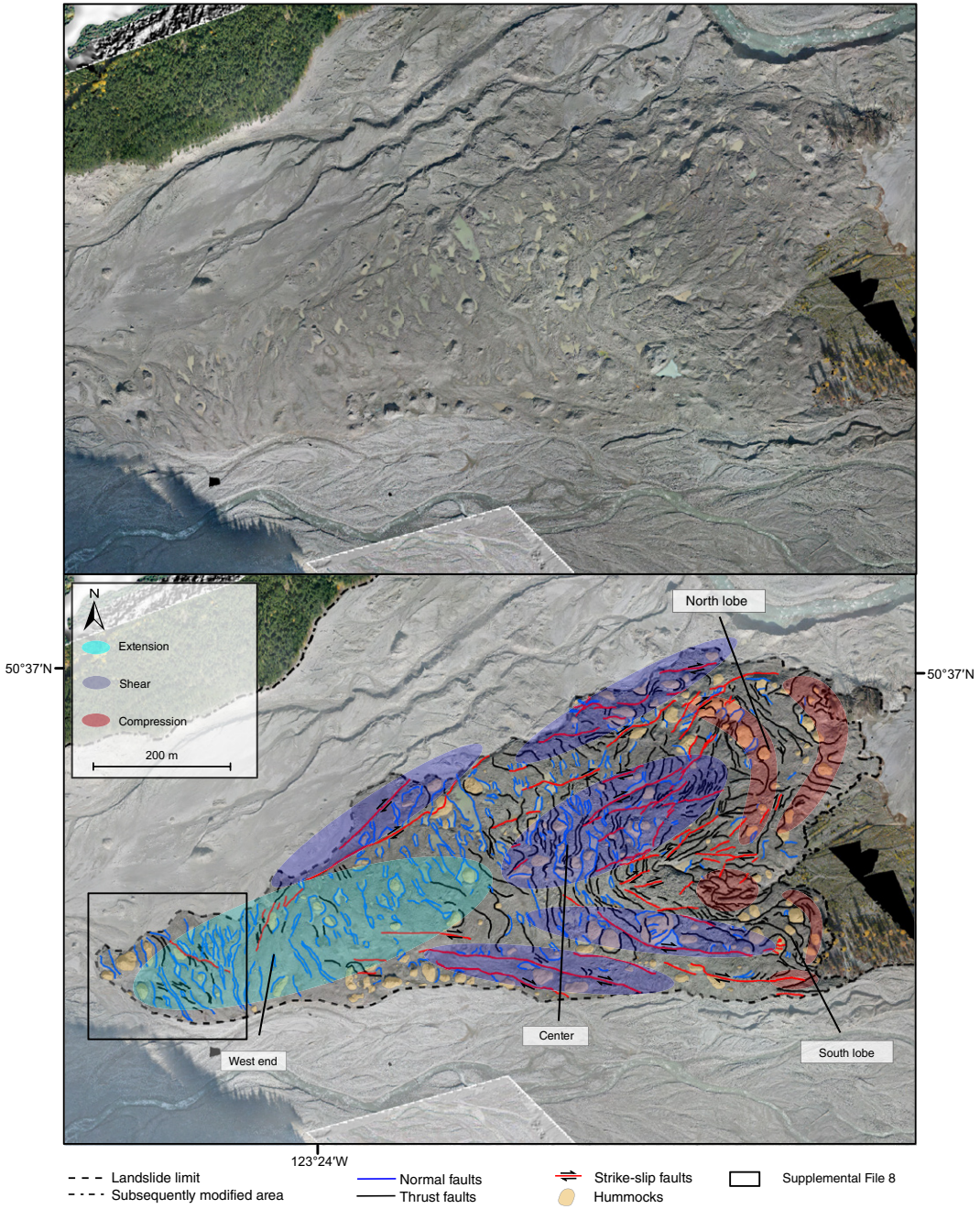

Figure 8. Orthophoto of the plug area, Mount Meager landslide (area 3). Structures indicate different stress regimes: extension (light blue) at the west corner of the plug; shear (purple) in the central part and at the sides; and compression (red) at the front and between the two lobes. Box indicates location of Supplemental File 8 (see footnote 8), which shows structures and deformation sequence.

Area 4: Distal Zone Up-Valley of the Campsite ("Distal Up")

Area 4 encompasses the marginal zone of the landslide between Lillooet River and the unaffected forest to the east, and is northwest of the British Columbia Forest Service campsite (Fig. 1). The distal-up area is 470 m wide and 450 m long (area 4 in Figs. 1 and 2). The maximum thickness of the debris is 4 m. Piles of trees up to 3 m high form the eastern edge of the landslide. Lillooet River sediments were entrained by the landslide in this area. The most distinctive feature in area 4 is a 2.5–4-m-high scarp, which marks the underlying, pre-landslide east bank of Lillooet River.

Two units of landslide debris are present in the distal-up area (Figs. 9A and 9B). Unit *a* is <1 m thick and consists mainly of mixed and woody debris facies, but includes hummocks of both block and entrained facies that were bulldozed to the margin of the deposit (Fig. 9A). Tree stems are oriented orthogonal to the flow direction and are in contact with standing, abraded, and tilted trees. At the river edge, entrained fluvial sediment was bulldozed into compressional ridges and hummocks.

Unit *b* is thicker and comprises debris similar to the deposits that form the plug, with meter-high hummocks and compressional ridges (Fig. 9A). In the northwestern part of area 4, unit *b* can be further subdivided into two different subunits. One has compressional ridges up to 3 m high and 20 m long and is in contact with the buried bank of Lillooet River. The other, which laps onto the first, has subdued ridges and lobes and some faults. Unit *a* flowed onto the terrace on which the Forest Service campsite is located, whereas unit *b* was stopped by it (Fig. 9B).

Moving downstream (southeast) in area 4, a fan-shaped lobe of thick debris covers the terrace and terminates in a 3–4-m-high front that is in contact with standing trees. Some trees were pushed forward and tilted back into the debris field by this lobe.

Farther downstream, at the southeastern end of area 4, Lillooet River has eroded the terrace to form a new bank. The contact between the river sediments and the landslide debris is exposed in the riverbank, and here the debris is 0.5–2 m thick.

Area 4: Interpretation

The deposit in area 4 reflects interactions with preexisting topography and different flow rheologies. The riverbank divided the flow in two: the water-rich phase (unit *a*) ran up over the bank, whereas the water-poor debris (unit *b*) was largely redirected and channeled by the bank. At the downstream end of area 4, unit *b* is in contact with, and laps onto, unit *a*.

The debris avalanche displaced Lillooet River water in area 4. Thus the fluid front is well developed here, extending as much as 180 m beyond the dense deposit. Eyewitnesses described a rush of muddy water along the logging road behind the campsite associated with this phase of the landslide (Guthrie et al., 2012a).

Area 5: Distal Zone Down-Valley of the Campsite ("Distal Down")

Area 5 is the most distal part of the landslide, located southeast (downstream) of the Forest Service campsite and extending from Lillooet River to the undisturbed forest on the east. The distal-down area is ~1000 m wide and 350 m long (area 5 in Figs. 1 and 2). The deposit thickness decreases from ~5–7 m to zero in the direction of flow.

We recognize two main depositional units (*a* and *b*) in area 5 (Figs. 10A and 10B). Unit *a* is the transition from a zone of dead drowned trees into woody debris, and then into a zone of sparse debris and small hummocks. In unit *a*, the number of standing trees decreases inward toward unit *b*. Some trees are tilted and their stems abraded to heights of 6 m, with pebbles and cobbles embedded in the wood. The zone of dead drowned trees with no debris (Fig. 10A) is 500 m wide and up to 200 m long with respect to the northeastern flow direction. An accumulation of woody debris, which lies west of the zone of dead trees, is up to 6 m thick and has a width of 8–100 m. Still farther west is an area of discontinuous debris with small (1–9 m^3) hummocks of block and entrained facies and sparse tree stems (Fig. 10B). The debris in this area occurs in several lobes, the largest of which is 20–180 m wide.

Unit *b* is a deposit of hummocky debris up to 7 m thick. It extends as much as 150 m outward (northeast) from Lillooet River (Fig. 10A). The hummocks are mainly block facies and have volumes of 100–120 m^3 (Fig. 10B). Areas between hummocks have a slightly ridged morphology, but the structure is not well expressed. This unit laps onto unit *a*; locally the two are separated by a scarp ~2 m high.

Area 5: Interpretation

The deposits in area 5 record a succession of events. A flood of water-rich material arrived first. It inundated the forest at the distal margin of the debris avalanche and left a frontal log jam and, just behind it, a zone of small hummocks (unit *a*). Water-poor debris arrived next, depositing unit *b* against the water-rich deposits. As was the case in area 4 upstream of the campsite, the front of the debris avalanche incorporated or displaced water from Lillooet River, sending unit *a* as much as 350 m beyond the limit of the denser material.

DISCUSSION

Detailed study of the facies and surface morphology of the 2010 Mount Meager debris avalanche allows us to infer emplacement mechanisms, the relative timing of phases, and flow rheology. The structure and form of the deposit differ along the landslide path, providing information on transport and depositional processes and the evolution of the debris avalanche. Our interpretation of the flow dynamics and flow separation is presented below, along with their hazard implications.

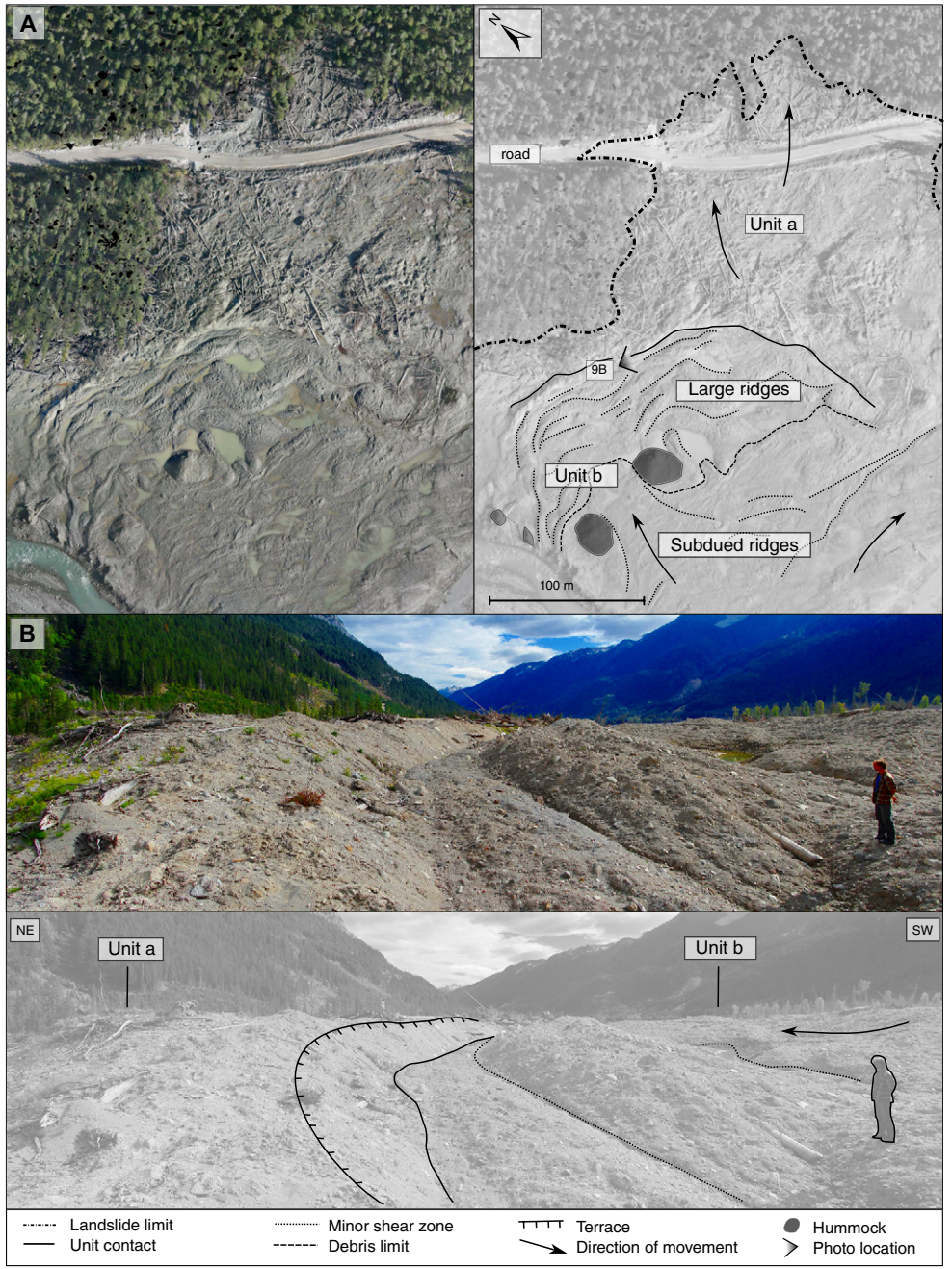

Figure 9. (A) Orthophoto of the distal part of the Mount Meager landslide deposit upstream of the unaffected Forest Service campsite (area 4), showing units *a* and *b*. Location of B is shown. (B) Partially buried terrace scarp showing the boundary between units *a* and *b*.

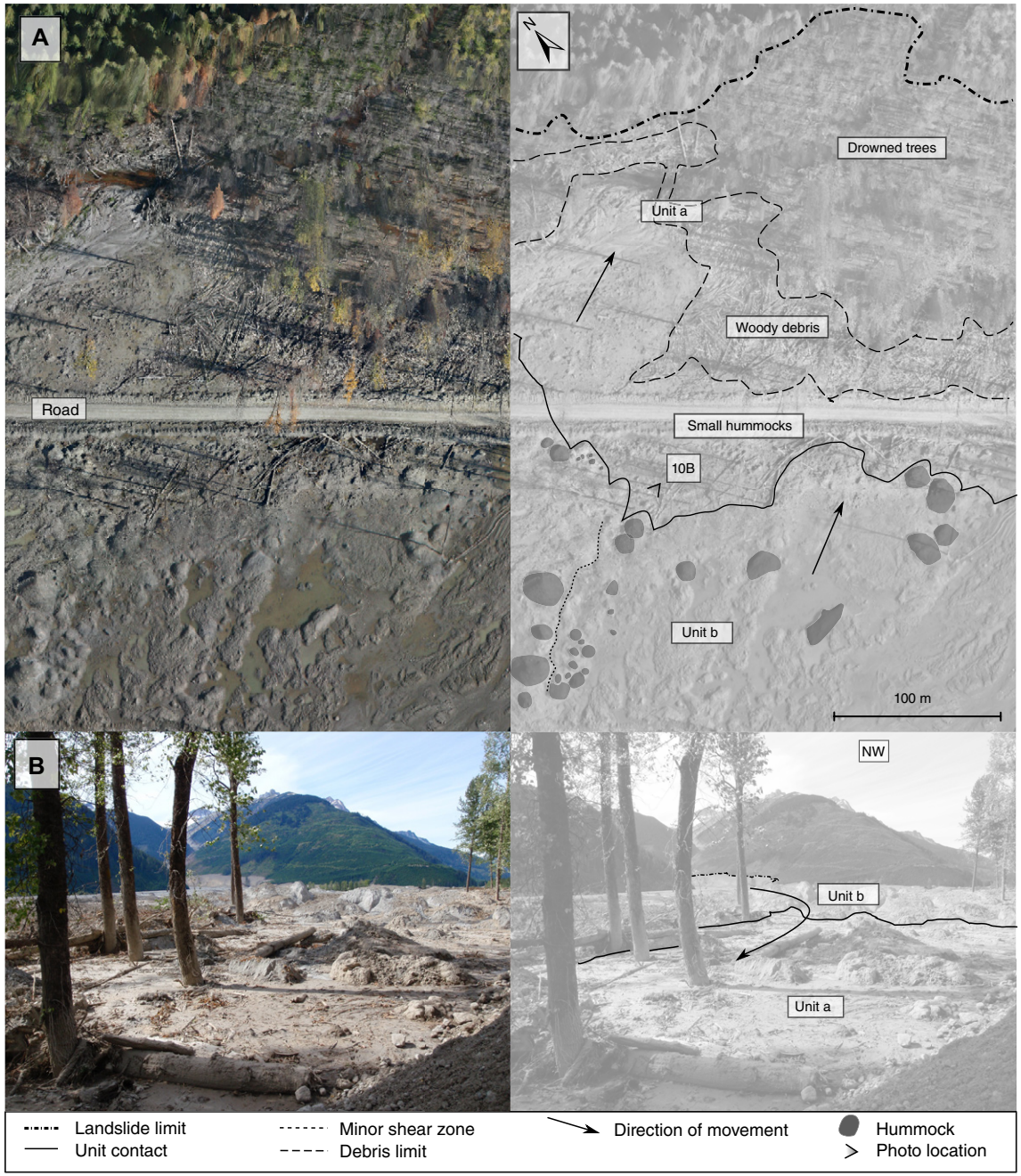

Figure 10. (A) Orthophoto of the distal part of the Mount Meager landslide deposit downstream of the unaffected Forest Service campsite (area 5) showing units, hummocks, shear zones, and the direction of movement. Location of B is shown. (B) Contact between thick hummocky debris (unit *b*) and the discontinuous debris veneer with small hummocks (unit *a*).

Lithology and Grain Size

The lithology of the landslide debris provides insight into its depositional processes. The distribution of altered material is particularly instructive. Altered materials are associated with block facies and sheared block facies streaks. Altered block and sheared block facies are more common at the downstream end of the plug than at the upstream end. Mud balls and altered sheared block facies streaks were also noted along the downstream margin of the terrace area. Conversely, the Meager barrier has less debris of the altered block and sheared block facies; it is primarily composed of very large gray porphyritic rhyodacite blocks within mixed material. We infer that this lithological zoning reflects the structure of the original rock mass in the source area: hydrothermally altered rock at the base of the source scarp and fresh rock typical of the volcanic plug higher up on the scarp.

The mixed material is dominantly silty clayey sand with clay percentages ranging from 5% to 8%. Altered sheared block facies samples may have up to 30% clay, whereas the fresh unaltered sheared block facies is 2%–5% clay (Fig. 4). The average clay content by facies is 6.1% mixed, 24.6% altered block, and 3.6% pulverized block. A mixing ratio of 12% altered to 88% pulverized is required to get 6.1% clay in the mixed facies. This simple analysis suggests that ~12% of the failed rock mass was hydrothermally altered. Furthermore, within the mixed material there is no apparent trend in the mean clay content from upstream to downstream, suggesting that the material became well mixed as it traversed Capricorn Creek.

Rheology Phases

There is evidence of multiple pulses of flow of diminishing magnitude over time, but the deposits can be generally classified into two main rheology types: water-poor and water-rich (Fig. 11). These two rheology types are, in reality, end members in what was a continuum. The water-poor end member produced thick debris avalanche–like deposits, with abundant large hummocks. Kinematic structures reveal sequential movement related to pulses in the emplacement process (Fig. 12A). The water-rich end member is responsible for a flood-like deposit with sparse tree stems amid standing trees with meter-high splash lines and trunk erosion, and has no significant lithic debris (Fig. 12B). This end member, however, transitions into woody debris, which in turn transitions into an area with hummocks morphologically similar to those of the debris flow and hyperconcentrated flow deposits. Structural discontinuities, including faults, shear zones, and compressional ridges, delineate zones with distinct internal morphological characteristics that are related to one of the two end members. However, the boundaries between these deposits are not sharp everywhere, suggesting gradual phase transitions (areas 4 and 5). Distinct debris lines indicate multiple pulses (areas 1 and 2) with different rheologies.

The water-rich phase is evident along the margins of the debris avalanche deposit, except at the front of the plug area. Water-rich flow deposits are overlain by, but extend beyond, the deposits of the water-poor phase. In the plug area (area 3), the debris terminates with a sharp front and there is no evidence of a leading water-rich phase, suggesting that the two phases followed different trajectories as they entered the Meager Creek–Lillooet River confluence area.

The two phases had different velocities and different paths that were controlled by the complex topography over which the debris avalanche traveled. The sinuous longitudinal form of Capricorn Creek valley (Fig. 1) resulted in centripetal and centrifugal forces that generated a marked separation of debris. The water-rich phase accelerated, achieving higher velocities and thus reaching farther up the valley sides, while the less-mobile water-poor core moved along the valley bottom. These differences in trajectory led to different deposits along Meager Creek and in Lillooet River valley.

Our evidence suggests that the water-rich phase preceded the water-poor phase, in contrast with the conclusion of Guthrie et al. (2012b) that a first, drier front came to rest in the plug area ~10 km from the source area and "the flow crossed the Lillooet River on both sides and over this plug" (p. 670). A water-rich phase followed by a water-poor phase is not unusual in debris flows and debris avalanches (cf. Oso landslide, Washington, USA; Iverson et al., 2015).

However, the water-rich slurries at the west end and margins of the plug suggest that some water-rich flows followed the emplacement of the plug. Copious water may have flowed from the source scar and remobilized part of the newly deposited material after the plug came to rest. It is thus difficult to distinguish a fluid tail contemporaneous with the debris avalanche from secondary debris mobilization by water flowing down Capricorn Creek.

Summary of the Event

Figure 13 summarizes our view of the 2010 Mount Meager debris avalanche in terms of rheology and velocity from its beginning to its end. The *x*-axis in the figure is the proportion of water and sediment in the flow, from debris avalanche to clear-water flood; the *y*-axis indicates both the strain rate and velocity. The different fields are based primarily on morphology. We postulate four stages in this history:

- Stage 1. The south flank of Mount Meager failed following infiltration of water generated by snowmelt and permafrost thaw into hydrothermally altered rock and colluvium on the lower part of the slope. In the first several seconds, the collapsed material behaved as a single mass and the motion was relatively slow, with an average speed of 4 m/s (Allstadt, 2013) (Fig. 14A).
- Stage 2. The failed mass accelerated rapidly, disaggregated, and spread as it started to flow down the valley of Capricorn Creek. High water pressure caused liquefaction and forced the water upward and outward, creating a mobile, water-rich frontal flow (Fig. 14B).

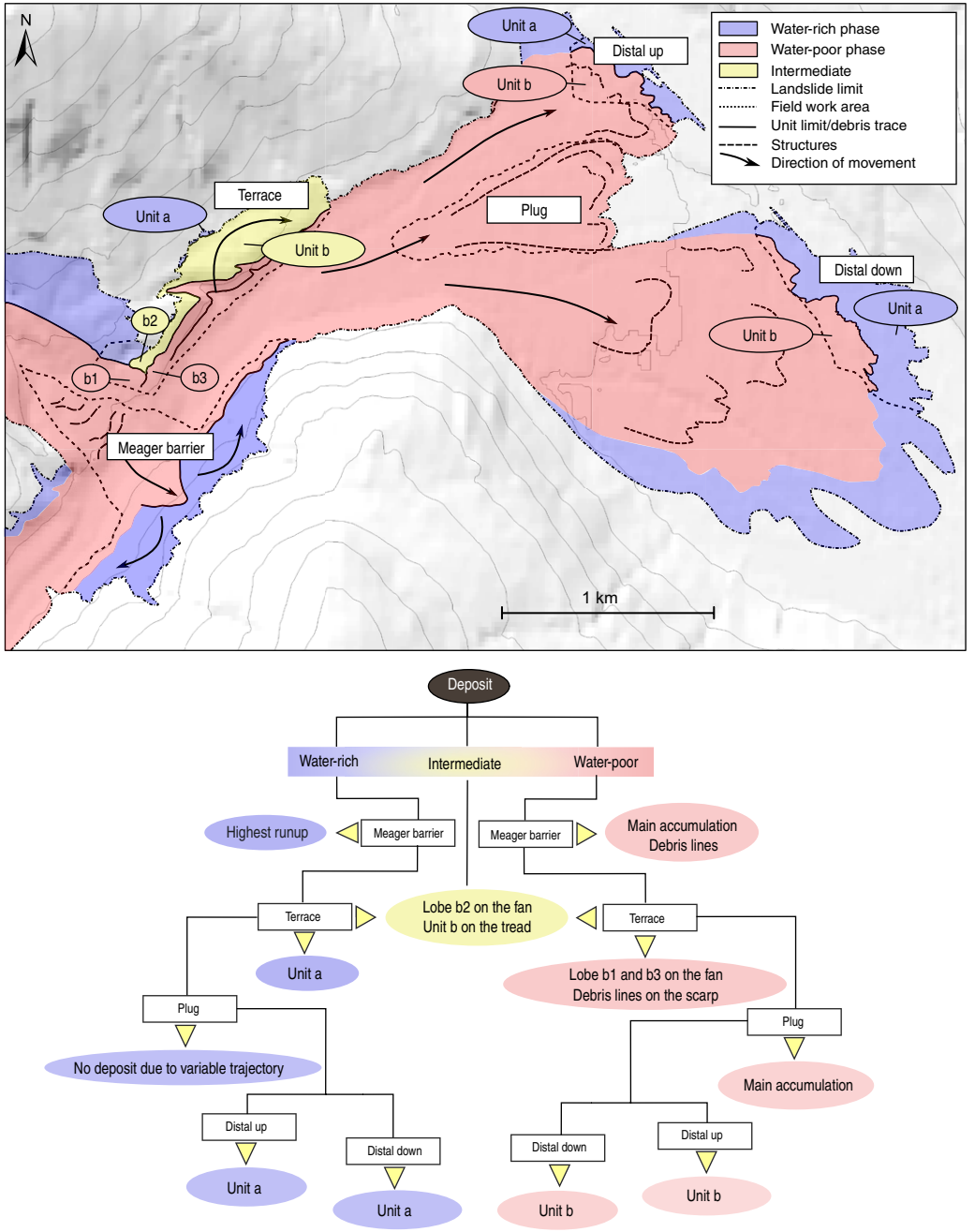

Figure 11. Top: Summary sketch map showing the distribution of water-rich and water-poor deposits of the Mount Meager landslide. Bottom: Flow chart summarizing the correlation between rheology phases, areas, and deposits. The water-rich phase produced the high debris line at the Meager barrier and deposited unit *a* in the terrace, distal up, and distal down areas. There are no traces of the water-rich phase in the plug area. The water-poor phase produced the lower debris line at the Meager barrier and left the thick body of debris in that area. It left the debris lines on the terrace scarp and unit *b* (lobes *b1* and *b3*) on the terrace fan and in the distal up and distal down areas. The plug was also deposited by the water-poor phase. Unit *b* on the terrace tread and lobe *b2* on the terrace fan are interpreted as deposited by an intermediate-water-content phase.

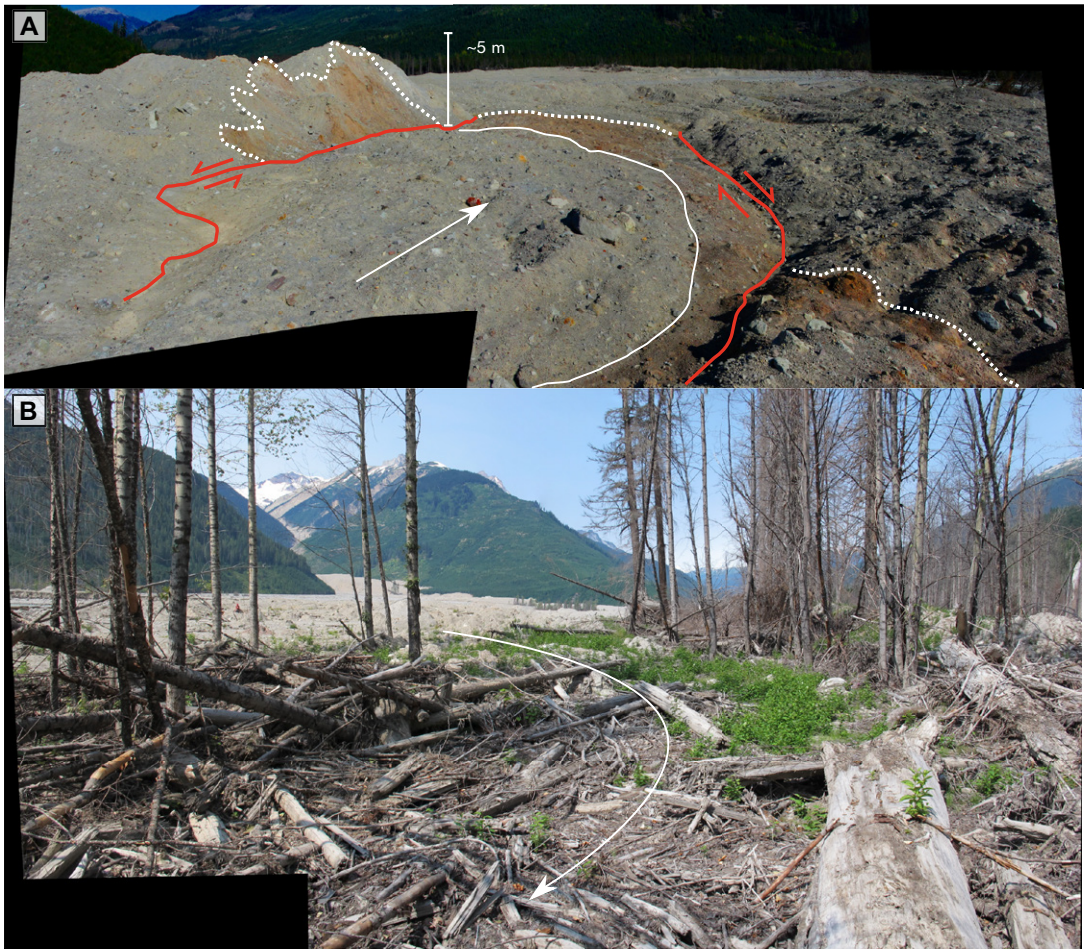

Figure 12. Rheology end-member deposits, Mount Meager landslide. (A) Thick debris, hummocks, and faults of the water-poor phase in area 3. The red line marks strike-slip faults; the white dotted lines delineate block and sheared block facies. (B) Woody debris and dead trees of the water-rich phase downstream of the unaffected Forest Service campsite. White arrow indicates the direction of movement.

- Stage 3. The water-rich flow accelerated and superelevated at the bends in Capricorn Creek valley, causing the high runups documented by Guthrie et al. (2012a, 2012b). It entered Meager Creek valley slightly in advance of the slower water-poor flow. Both ran up the opposing valley wall and turned back toward the opposite side of the valley. The water-rich phase split in two lobes (Fig. 14C). One lobe overrode the terrace (area 2) and then flowed back toward Meager Creek to affect area 5 down-valley of the Forest Service campsite. A second lobe was deflected by the terrace and followed a straight trajectory to area 4 up-valley of the campsite. Both lobes decelerated, leaving thin debris, small hummocks, and standing water, indicative of further flow separation. The most distal deposit of the water-rich phase in areas 4 and 5 shows evidence of extreme water content as the flow displaced and incorporated water from Lillooet River.
- Stage 4. After impacting the southeast wall of Meager Creek valley, the water-poor phase deposited thick debris in the Meager Creek–Lillooet River confluence area (Fig. 14D). During final emplacement, it separated into three lobes: a central, less mobile one (area 3) and two lateral wings that flowed farther, crossing Lillooet River and leaving the water-poor deposits in areas 4 and 5. As the water-poor phase decelerated and came to rest, it developed ductile-brittle deformation structures. It did not travel as far as the water-rich phase.

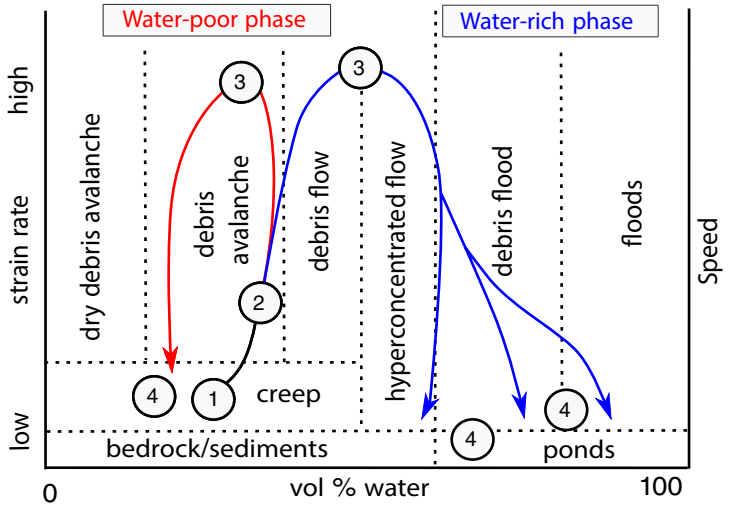

Figure 13. Conceptual diagram showing stages in the evolution of the Mount Meager debris avalanche. (1) The south flank of Mount Meager fails. (2) The rock mass breaks up, spreads, and liquefies as it begins to accelerate down Capricorn Creek valley. Water escapes from beneath the debris avalanche, forming the advance water-rich phase (blue line); the bulk of the mass, in comparison, is relatively dry (red line). Although the two phases interact, they follow different paths and leave separate deposits. (3) Both phases achieve very high velocities before impacting the south valley wall of Meager Creek. They decelerate as they spread up and down Meager Creek and into Lillooet River valley. (4) Final deceleration and cessation of flow.

Although the water-rich and water-poor phases had different trajectories due to their differences in volumes and velocities, they did not behave totally independently. The presence of intermediate deposits suggests that they interacted. Furthermore, their separation in time was minor, perhaps only seconds.

The scenario outlined above is consistent with an analysis of seismic records of the landslide by Allstadt (2013). She concluded that "there is even a hint of what could be interpreted as two separate surges visible in the vertical component of the force-time function. The vertical component of the force … has a shorter duration than the eastward component and is followed by a second smaller upward pulse" (p. 15). The multiple debris lines on the valley sides, however, suggest more than two surge waves; some may not have been large enough to generate clear seismic signals.

Hazard Implications

Transformation of a dry debris avalanche into a saturated debris flow has been inferred for many events (Palmer and Neall, 1989; Vallance and Scott, 1997; Capra and Macias, 2000; Scott et al., 2002; Tost et al., 2014). In the case of the Mount Meager event, the transformation was partial, and multiple rheologies coexisted, with different mobilities, velocities, and trajectories. Our observations show that debris avalanches can be multiphase events with debris avalanche, debris flow, hyperconcentrated flow, debris flood, and flood-like components or phases (Fig. 13). This complexity may be more common than presently thought and may apply to other debris avalanche events. Here, different rheologies were clearly expressed in the deposit textures because the high sinuosity of the valley caused extreme separation of water-rich and water-poor phases. Also, the photo documentation immediately after the event allowed us to differentiate ephemeral water-rich deposits and flow traces that are not preserved in older events.

Numerical modeling of debris avalanches takes into account only dry granular material (Pudasaini and Hutter, 2003; Zahibo et al., 2010), and the models typically are single phase (Takahashi, 2007; Pudasaini, 2011). Only simplified, two-phase models traditionally are used for debris flows (Iverson, 1997; Pudasaini et al., 2005; Jakob et al., 2013). Recently, Pudasaini (2012) and Pudasaini and Krautblatter (2014) have proposed a more complete two-phase model for debris flows and debris avalanches that simulates the separation of a fluid front, drier core, and fluid tail.

The complexity of the 2010 Mount Meager debris avalanche highlights the difficulties of modeling such events and assessing the risk they pose to down-valley populations and infrastructure. The separation of water-poor and water-rich phases in complex topography has to be simulated to reproduce the different deposit types and the runout of each phase.

SUMMARY AND CONCLUSIONS

Field evidence and detailed geomorphic mapping of the 2010 Mount Meager landslide allowed us to document the development of multiple rheology phases with different mobilities and trajectories. As the collapsed mass disaggregated and started to flow along Capricorn Creek, it separated into a faster water-rich phase and a slower water-poor phase. The water-rich phase caromed down Capricorn Creek, ran high up the southeastern wall of Meager Creek valley, and overtopped a terrace on the opposite side of the valley, while the water-poor phase was more confined to the valley floor. The shapes of Capricorn and Meager Creek valleys contributed to the phase separation and deposit emplacement. The water-rich phase left the most distal deposit, but its deposit is not observed everywhere at the distal margin because the flow separated and was deflected by the topography. The less-mobile, water-poor phase left a continuous deposit.

Lithological zones in the deposit preserve the original distribution of rock in the source area, with hydrothermally altered rock derived from the base of the scar reaching the distal limit of the debris avalanche and gray rhyodacite rock higher on the flank of Mount Meager dominating more proximal deposits. Grain-size analysis and rough mixing estimates suggest that ~12% of the failed rock mass was hydrothermally altered.

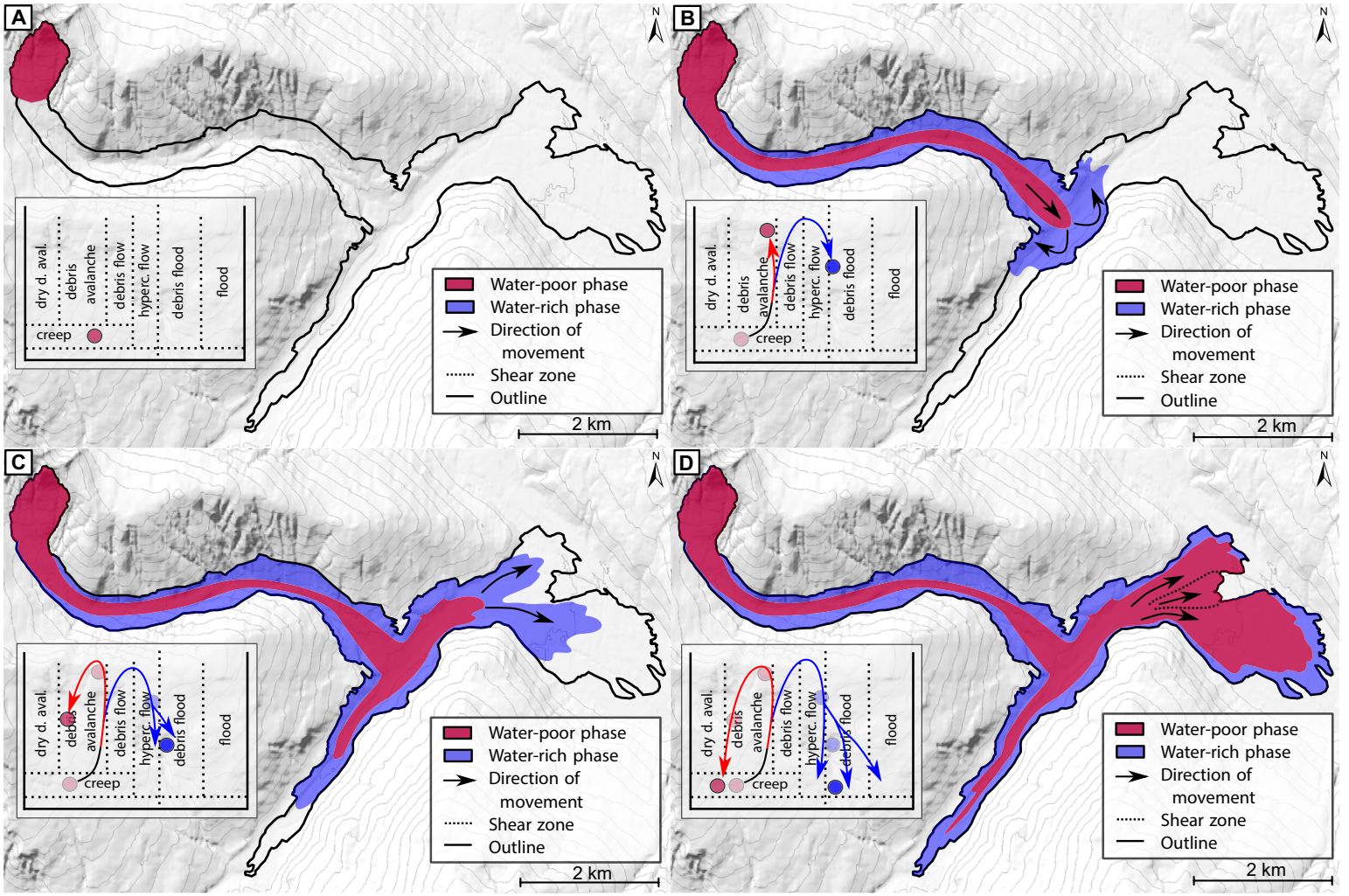

Figure 14. Schematic diagram showing the evolution of the Mount Meager debris avalanche with inferred rheological behavior. (A) At initiation, the collapsed material behaves as a single phase. (B) The water-rich phase forms as the debris avalanche moves down the valley of Capricorn Creek. Upon reaching Meager Creek, it runs 270 m up the south valley wall. (C) It then flows both up and down Meager Creek valley. (D) The water-rich phase travels farther than the water-poor phase. The latter leaves a thicker deposit, which displays deformation structures that develop during final emplacement. d. aval.—debris avalanche; hyperc.—hyperconcentrated.

Finally, this event raises new challenges for multi-rheology phase modeling of debris avalanches and hazard mapping. There were no fatalities in this particular event, but lack of understanding of the complex behavior of such landslides could result in inaccurate hazard assessment, placing populations at risk from catastrophic rock slope failures.

ACKNOWLEDGMENTS

We thank Engielle Paguican for taking the helicopter photos used for the SfM processing. Diego Masera, Mirko Francioni, Nancy Calhoun, and Hazel Wong assisted with field work. Discussions with Patrick Englehardt, Carie-Ann Lau, Snowy Haiblen, Libby Griffin, and Tatum Herrero helped us formulate some of our ideas, and we thank Fran van Wyk de Vries and Cat Lit for manuscript improvement. We thank Tim Davies and Lucia Capra

for the paper review. Financial support for the research was provided by geoNatHaz (EU-Canada Co-operation Project in Higher Education, Training and Youth) and the Region Auvergne, France.

REFERENCES CITED

Allstadt, K., 2013, Extracting source characteristics and dynamics of the August 2010 Mount Meager landslide from broadband seismograms: Journal of Geophysical Research: Earth Surface, v. 118, p. 1472–1490, doi:10.1002/jgrf.20110.

Bernard, B., van Wyk de Vries, B., Barba, D., Leyrit, H., Robin, C., Alcaraz, S., and Samaniego, P., 2008, The Chimborazo sector collapse and debris avalanche: Deposit characteristics as evidence of emplacement mechanisms: Journal of Volcanology and Geothermal Research, v. 176, p. 36–43, doi:10.1016/j.jvolgeores.2008.03.012.

Bovis, M., and Evans, S.G., 1996, Extensive deformations of rock slopes in southern Coast Mountains, southwest British Columbia, Canada: Engineering Geology, v. 44, p. 163–182, doi:10.1016/S0013-7952(96)00068-3.

Bovis, M., and Jakob, M., 2000, The July 29, 1998, debris flow and landslide dam at Capricorn Creek, Mount Meager Volcanic Complex, southern Coast Mountains, British Columbia: Canadian Journal of Earth Sciences, v. 37, p. 1321–1334, doi:10.1139/e00-042.

Bruce, I., and Cruden, D.M., 1977, The dynamics of the Hope slide: Bulletin of the International Association of Engineering Geology, v. 16, p. 94–98, doi:10.1007/BF02591458.

Capra, L., and Macias, J.L., 2000, Pleistocene cohesive debris flows at Nevado de Toluca Volcano, central Mexico: Journal of Volcanology and Geothermal Research, v. 102, p. 149–167, doi:10.1016/S0377-0273(00)00186-4.

Carter, N.M., 1932, Exploration in the Lillooet River watershed: Canadian Alpine Journal, v. 21, p. 8–18.

Clague, J.J., Evans, S.G., Rampton, V.N., and Woodsworth, G.J., 1995, Improved age estimates for the White River and Bridge River tephras, western Canada: Canadian Journal of Earth Sciences, v. 32, p. 1172–1179, doi:10.1139/e95-096.

Coe, J.A., Baum, R.L., Allstadt, K.E., Kochevar, B.F, Jr., Schmitt, R.G., Morgan, M.L., White, J.L., Stratton, B.T., Hayashi, T.A., and Kean, J.K., 2016, Rock-avalanche dynamics revealed by large-scale field mapping and seismic signals at a highly mobile avalanche in the West Salt Creek valley, western Colorado: Geosphere, v. 12, p. 607–631, doi:10.1130/GES01265.1.

Cruden, D.M., and Krahn, J., 1973, A reexamination of the geology of the Frank Slide: Canadian Geotechnical Journal, v. 10, p. 581–591, doi:10.1139/t73-054.

Cruden, D.M., and Martin, D.K., 2007, Before Frank slide: Canadian Geotechnical Journal, v. 44, p. 765–780, doi:10.1139/t07-030.

Finn, C.A., Sisson, T.W., and Deszcz-Pan, M., 2001, Aerogeophysical measurements of collapse-prone hydrothermally altered zones at Mount Rainier volcano: Nature, v. 409, p. 600–603, doi:10.1038/35054533.

Fonstad, M.A., Dietrich, J.T., Courville, B.C., Jensen, J.L., and Carbonneau, P.E., 2013, Topographic structure from motion: A new development in photogrammetric measurement: Earth Surface Processes and Landforms, v. 38, p. 421–430, doi:10.1002/esp.3366.

Friele, P., and Clague, J.J., 2004, Large Holocene landslides from Pylon Peak, southwestern British Columbia: Canadian Journal of Earth Sciences, v. 41, p. 165–182, doi:10.1139/e03-089.

Friele, P., and Clague, J.J., 2009, Paraglacial geomorphology of Quaternary volcanic landscapes in the southern Coast Mountains, British Columbia, *in* Knight, J., and Harrison, S., eds., Periglacial and Paraglacial Processes and Environments: Geological Society London Special Publication 320, p. 219–233, doi:10.1144/SP320.14.

Friele, P., Clague, J.J., Simpson, K., and Stasiuk, M., 2005, Impact of a Quaternary volcano on Holocene sedimentation in Lillooet River valley, British Columbia: Sedimentary Geology, v. 176, p. 305–322, doi:10.1016/j.sedgeo.2005.01.011.

Friele, P., Jakob, M., and Clague, J., 2008, Hazard and risk from large landslides from Mount Meager volcano, British Columbia, Canada: Georisk: Assessment and Management of Risk for Engineered Systems and Geohazards, v. 2, p. 48–64, doi:10.1080/17499510801958711.

Glicken, H.X., 1991, Sedimentary architecture for large volcanic debris avalanches, *in* Smith, G.A., and Fisher, R.V., eds., Sedimentation in Volcanic Settings: Society of Economic Paleontologists and Mineralogists Special Publication 45, p. 99–106, doi:10.2110/pec.91.45.0099.

Glicken, H.X., 1996, Rockslide-debris avalanche of May 18, 1980, Mount St. Helens volcano, Washington: U.S. Geological Survey Open-File Report 96-677, 90 p., 5 plates, http://pubs.usgs.gov/of/1996/0677/.

Guthrie, R.H., Friele, P., Allstadt, K., Roberts, N., Evans, S.G., Delaney, K.B., Roche, D., Clague, J.J., and Jakob, M., 2012a, The 6 August 2010 Mount Meager rock slide–debris flow, Coast Mountains, British Columbia: Characteristics, dynamics, and implications for hazard and risk assessment: Natural Hazards and Earth System Sciences, v. 12, p. 1277–1294, doi:10.5194/nhess-12-1277-2012.

Guthrie, R.H., Friele, P., Allstadt, K., Roberts, N., Evans, S.G., Delaney, K.B, Roche, D., Clague, J.J., Jakob, M., and Cronmiller, D., 2012b, The August 06, 2010 Mount Meager rock slide-debris flow, Coast Mountains, British Columbia, *in* Eberhardt, E., et al., eds., Landslides and Engineered Slopes: Protecting Society through Improved Understanding: London, Taylor & Francis Group, v. 48, p. 665–674.

Hickson, C.J., Russell, J.K., and Stasiuk, M.V., 1999, Volcanology of the 2350 B.P. eruption of Mount Meager Volcanic Complex, British Columbia, Canada: Implications for hazards from eruptions in topographically complex terrain: Bulletin of Volcanology, v. 60, p. 489–507, doi:10.1007/s004450050247.

Holm, K., Bovis, M., and Jakob, M., 2004, The landslide response of alpine basins to post–Little Ice Age glacial thinning and retreat in southwestern British Columbia: Geomorphology, v. 57, p. 201–216, doi:10.1016/S0169-555X(03)00103-X.

Iverson, R.M., 1997, The physics of debris flows: Reviews of Geophysics, v. 35, p. 245–296, doi:10.1029/97RG00426.

Iverson, R.M., George, D.L., Allstadt, K., Reid, M.E., Collins, B.D., Vallance, J.W., Schilling, S.P., Godt, J.W., Cannon, C.M., Magirl, C.S., Baum, R.L., Coe, J.A., Schulz, W.H., and Bower, J.B., 2015, Landslide mobility and hazards: Implications of the 2014 Oso disaster: Earth and Planetary Science Letters, v. 412, p. 197–208, doi:10.1016/j.epsl.2014.12.020.

Jakob, M., 1996, Morphometric and geotechnical controls on debris flow frequency and magnitude, southern Coast Mountains, British Columbia [Ph.D. thesis]: Vancouver, University of British Columbia, 242 p.

Jakob, M., McDougall, S., Weatherly, H., and Ripley, N., 2013, Debris-flow simulations on Cheekye River, British Columbia: Landslides, v. 10, p. 685–699, doi:10.1007/s10346-012-0365-1.

James, M.R., and Robson, S., 2012, Straightforward reconstruction of 3D surfaces and topography with a camera: Accuracy and geoscience application: Journal of Geophysical Research, v. 117, F03017, doi:10.1029/2011JF002289.

Jordan, P., 1994, Debris flows in the southern Coast Mountains, British Columbia: Dynamic behaviour and physical properties [Ph.D. thesis]: Vancouver, University of British Columbia, 272 p.

Kelfoun, K., 2011, Suitability of simple rheological laws for the numerical simulation of dense pyroclastic flows and long-runout volcanic avalanches: Journal of Geophysical Research, v. 116, B08209, doi:10.1029/2010JB007622.

Mathews, W.H., and McTaggart, K.C., 1969, The Hope landslide, British Columbia: Proceedings of the Geological Association of Canada, v. 20, p. 65–75.

Micheletti, N., Chandler, J.H., and Lane, S.N., 2015, Structure from Motion (SfM) photogrammetry, *in* Cook, S.J., et al., eds., Geomorphological Techniques (online edition): London, British Society for Geomorphology, section 2.2, 12 p.

Mokievsky-Zubok, O., 1977, Glacier-caused slide near Pylon Peak, British Columbia: Canadian Journal of Earth Sciences, v. 15, p. 1039–1052.

Moretti, L., Allstadt, K., Mangeney, A., Capdeville, Y., Stutzmann, E., and Bouchut, F., 2015, Numerical modeling of the Mount Meager landslide constrained by its force history derived from seismic data: Journal of Geophysical Research: Solid Earth, v. 120, p. 2579–2599, doi:10.1002/2014JB011426.

Paguican, E.M.R., van Wyk de Vries, B., and Lagmay, A.M.F., 2014, Hummocks: How they form and how they evolve in rockslide-debris avalanches: Landslides, v. 11, p. 67–80, doi:10.1007/s10346-012-0368-y.

Palmer, B.A., and Neall, V.E., 1989, The Murimotu Formation: 9500 year old deposits of a debris avalanche and associated lahars, Mount Ruapehu, North Island, New Zealand: New Zealand Journal of Geology and Geophysics, v. 32, p. 477–486, doi:10.1080/00288306.1989.10427555.

Plafker, G., and Ericksen, G.E., 1978, Nevado Huascarán avalanches, Peru, *in* Voight, B., ed., Rockslides and Avalanches: Natural Phenomenon: Amsterdam, Elsevier, v. 1, p. 277–314, doi:10.1016/B978-0-444-41507-3.50016-7.

Pola, A., Crosta, G.B., Fusi, N., and Castellanza, R., 2014, General characterization of the mechanical behaviour of different volcanic rocks with respect to alteration: Engineering Geology, v. 169, p. 1–13, doi:10.1016/j.enggeo.2013.11.011.

Pudasaini, S.P., 2011, Some exact solutions for debris and avalanche flows: Physics of Fluids, v. 23, 043301, doi:10.1063/1.3570532.
Pudasaini, S.P., 2012, A general two-phase debris flow model: Journal of Geophysical Research, v. 117, F03010, doi:10.1029/2011JF002186.
Pudasaini, S.P., and Hutter, K., 2003, Rapid shear flows of dry granular masses down curved and twisted channels: Journal of Fluid Mechanics, v. 495, p. 193–208, doi:10.1017/S0022112003006141.
Pudasaini, S.P., and Krautblatter, M., 2014, A two-phase mechanical model for rock-ice avalanches: Journal of Geophysical Research: Earth Surface, v. 119, p. 2272–2290, doi:10.1002/2014JF003183.
Pudasaini, S.P., Wang, Y., and Hutter, K., 2005, Modelling debris flows down general channels: Natural Hazards and Earth System Sciences, v. 5, p. 799–819, doi:10.5194/nhess-5-799-2005.
Read, P.B., 1977, Meager Creek volcanic complex, southwestern British Columbia, *in* Current Research, Part A: Geological Survey of Canada Paper 77–1A, p. 277–281.
Read, P.B., 1979, Geology, Meager Creek geothermal area, British Columbia: Geological Survey of Canada Open File 603, 1 sheet, scale 1:20,000.
Read, P.B., 1990, Mount Meager Complex, Garibaldi Belt, southwestern British Columbia: Geoscience Canada, v. 17, p. 167–170.
Reid, M.E., and Brien, D.L., 2006, Assessing massive flank collapse at stratovolcanoes using 3-D slope stability analysis, *in* Evans, S.G., et al., eds., Landslides from Massive Rock Slope Failure: Dordrecht, Springer, p. 445–458, doi:10.1007/978-1-4020-4037-5_24.
Remondino, F., Spera, M.G., Nocerino, E., Menna, F., and Nex, F., 2014, State of the art in high density image matching: The Photogrammetric Record, v. 29, p. 144–166, doi:10.1111/phor.12063.
Roche, A.D., Guthrie, R.H., Roberts, N.J., Ellis, E., and Friele, P., 2011, Once more into the breach: A forensic analysis of the August 2010 landslide dam outburst flood at Meager Creek, BC, *in* Proceedings of 5th Canadian Conference on Geotechnique and Natural Hazards, Kelowna, British Columbia, 15–17 May: Canadian Geotechnical Society, 10 p.
Roverato, M., Cronin, S., Procter, J., and Capra, L., 2014, Textural features as indicators of debris avalanche transport and emplacement, Taranaki volcano: Geological Society of America Bulletin, v. 120, p. 3–18, doi:10.1130/B30946.1.
Scott, K.M., Macias, J.L., Vallance, J.W., Naranjo, J.A., Rodriguez-Elizarraras, S.R., and McGeehin, J.P., 2002, Catastrophic debris flows transformed from landslides in volcanic terrains: Mobility, hazard assessment, and mitigation strategy: U.S. Geological Survey Professional Paper 1630, 59 p.
Shea, T., and van Wyk de Vries, B., 2008, Structural analysis and analogue modeling of the kinematics and dynamics of rockslide avalanches: Geosphere, v. 4, p. 657–686, doi:10.1130/GES00131.1.
Shea, T., and van Wyk de Vries, B., 2010, Collapsing volcanoes: The sleeping giants' threat: Geology Today, v. 26, p. 72–77, doi:10.1111/j.1365-2451.2010.00750.x.
Siebert, L., 2002, Landslides resulting from structural failure of volcanoes: Reviews in Engineering Geology, v. 15, p. 209–235, doi:10.1130/REG15-p209.
Simpson, K.A., Stasiuk, M., Shimamura, K., Clague, J.J., and Friele, P., 2006, Evidence for catastrophic volcanic debris flows in Pemberton Valley, British Columbia: Canadian Journal of Earth Sciences, v. 689, p. 679–689, doi:10.1139/E06-026.
Smith, M.W., Carrivick, J.L., and Quincey, D.J., 2015, Structure from motion photogrammetry in physical geography: Progress in Physical Geography, v. 40, p. 247–275, doi:10.1177/0309133315615805.
Snavely, N., Seitz, S.N., and Szeliski, R., 2008, Modeling the world from internet photo collections: International Journal of Computer Vision, v. 80, p. 189–210, doi:10.1007/s11263-007-0107-3.
Soil Survey Division Staff, 1993, Soil survey manual: U.S. Department of Agriculture Soil Conservation Service Agricultural Handbook 18, https://www.nrcs.usda.gov/wps/portal/nrcs/detail/soils/ref/?cid=nrcs142p2_054262.
Takahashi, T., 2007, Debris Flow: Mechanics, Prediction and Countermeasures: New York, Taylor and Francis, 440 p., doi:10.1201/9780203946282.
Takarada, S., Ui, T., and Yamamoto, Y., 1999, Depositional features and transportation mechanism of valley-filling Iwasegawa and Kaida debris avalanches, Japan: Bulletin of Volcanology, v. 60, p. 508–522, doi:10.1007/s004450050248.
Tost, M., Cronin, S.J., Procter, J.N., Smith, I.E.M., Neall, V.E., and Price, R.C., 2014, Impacts of catastrophic volcanic collapse on the erosion and morphology of a distal fluvial landscape: Hautapu River, Mount Ruapehu, New Zealand: Geological Society of America Bulletin, v. 127, p. 266–280, doi:10.1130/B31010.1.
Ui, T., Takarada, S., and Yoshimoto, M., 2000, Debris avalanches, *in* Sigurdsson, H., ed., Encyclopedia of Volcanoes: San Diego, Academic Press, p. 617–626.
Vallance, W., and Scott, K.M., 1997, The Osceola mudflow from Mount Rainier: Sedimentology and hazard implications of a huge clay-rich debris flow: Geological Society of America Bulletin, v. 109, p. 143–163, doi:10.1130/0016-7606(1997)109<0143:TOMFMR>2.3.CO;2.
van Wyk de Vries, B., and Davies, T., 2015, Landslides, debris avalanches, and volcanic gravitational deformation, *in* Sigurdsson, H., et al., eds., Encyclopedia of Volcanoes (second edition): London, Academic Press, p. 665–685, doi:10.1016/B978-0-12-385938-9.00038-9.
van Wyk de Vries, B., and Delcamp, A., 2015, Volcanic debris avalanches, *in* Davies, T., ed., Landslide Hazards, Risks, and Disasters: Amsterdam, Elsevier, p. 131–157, doi:10.1016/B978-0-12-396452-6.00005-7.
van Wyk de Vries, B., and Francis, P.W., 1997, Catastrophic collapse at stratovolcanoes induced by gradual volcano spreading: Nature, v. 387, p. 387–390, doi:10.1038/387387a0.
Westoby, M.J., Brasington, J., Glasser, N.F., Hambrey, M.J., and Reynolds, J.M., 2012, 'Structure-from-Motion' photogrammetry: A low-cost, effective tool for geoscience applications: Geomorphology, v. 179, p. 300–314, doi:10.1016/j.geomorph.2012.08.021.
Zahibo, N., Pelinovsky, E., Talipova, T., and Nikolkina, I., 2010, Savage-Hutter model for avalanche dynamics in inclined channels: Analytical solutions: Journal of Geophysical Research, v. 115, B03402, doi:10.1029/2009JB006515.